



Cite this: *RSC Adv.*, 2023, 13, 3652

Organic binary charge-transfer compounds of 2,2':6',2'':6'',6-trioxotriphenylamine and a pyrene-annulated azaacene as donors†

Rajorshi Das,^a Michael Linseis,^a Stefan M. Schupp,^b Franciska S. Gogesch,^a Lukas Schmidt-Mende^{id}^b and Rainer F. Winter^{id}^{*a}

Three binary charge-transfer (CT) compounds resulting from the donor 2,2':6',2'':6'',6-trioxotriphenylamine (TOTA) and the acceptors F₄TCNQ and F₄BQ and of a pyrene-annulated azaacene (PAA) with the acceptor F₄TCNQ are reported. The identity of these CT compounds are confirmed by single-crystal X-ray diffraction as well as by IR, UV-vis-NIR and EPR spectroscopy. X-ray diffraction analysis reveals a 1:1 stoichiometry for TOTA·F₄TCNQ, a 2:1 donor:acceptor ratio in (TOTA)₂·F₄BQ, and a rare 4:1 stoichiometry in (PAA)₄·F₄TCNQ, respectively. Metrical parameters of the donor (D) and acceptor (A) constituents as well as IR spectra indicate full CT in TOTA·F₄TCNQ, partial CT in (TOTA)₂·F₄BQ and only a very modest one in (PAA)₄·F₄TCNQ. Intricate packing motifs are present in the crystal lattice with encaged, π -stacked (F₄TCNQ[−])₂ dimers in TOTA·F₄TCNQ or mixed D/A stacks in the other two compounds. Their solid-state UV-vis-NIR spectra feature CT transitions. The CT compounds with F₄TCNQ are electrical insulators, while (TOTA)₂·F₄BQ is weakly conducting.

Received 17th November 2022

Accepted 18th January 2023

DOI: 10.1039/d2ra07322f

rsc.li/rsc-advances

Introduction

Ever since the first report on the charge-transfer compound TTF⁺·TCNQ[−] (TTF = tetrathiafulvalene, TCNQ = tetracyanoquinodimethane) with metal-like conductivity,¹ organic charge-transfer (CT) systems D^{δ+}·A^{δ−}, composed of a donor (D) and an acceptor (A), have attracted a great deal of attention.^{2–6} Compounds of this type can act as good electrical conductors or components of ambipolar semiconductors³ and may show other intriguing properties including strong electron–phonon coupling,^{7,8} photoelectricity,^{9–13} ferromagnetism,¹⁴ antiferromagnetism,¹⁵ or luminescence.^{16–19} The degree of charge-transfer between the D and A components tends to increase with a decreasing energy difference between the lowest unoccupied molecular orbital LUMO of the acceptor A and the highest occupied molecular orbital HOMO of the donor D. Such information can be retrieved by quantum chemical calculations²⁰ or, on an experimental basis, from their electrochemical reduction or oxidation potentials, respectively.³ These data therefore provide useful guidelines to adjust the likely degree of CT and aid in the purposeful design of CT compounds. For

example, the combination of a strong donor with a strong acceptor usually leads to the formation of a CT compound D⁺·A[−] with a full transfer of charge (type-I, Fig. 1). This class of compounds may show strong ferromagnetism, but is often associated with only poor charge-transport capabilities.^{15,21,22}

The properties of D–A-based CT compounds do, however, not only depend on the degree of charge-transfer, but also on the stoichiometric ratio D:A and on intermolecular D/D, A/A and D/A interactions in the crystal lattice. The various modes

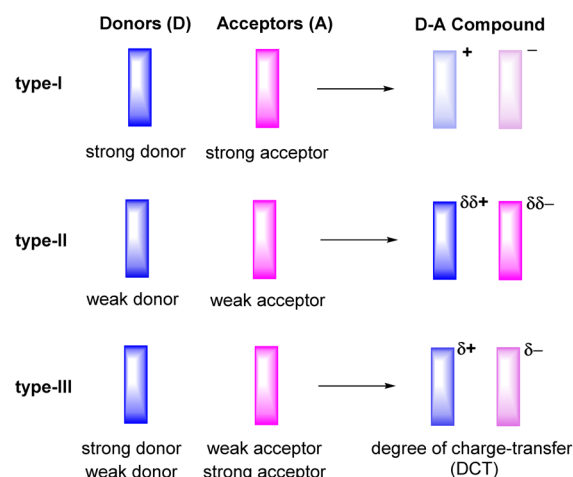


Fig. 1 Degrees of charge-transfer for varieties of donor–acceptor (D–A) based organic CT compounds.

^aFachbereich Chemie, Universität Konstanz, Universitätsstrasse 10, 78457 Konstanz, Germany. E-mail: rainer.winter@uni-konstanz.de

^bFachbereich Physik, Universität Konstanz, Universitätsstrasse 10, 78457 Konstanz, Germany

† Electronic supplementary information (ESI) available. CCDC 2220394, 2220397 and 2220398. For ESI and crystallographic data in CIF or other electronic format see DOI: <https://doi.org/10.1039/d2ra07322f>



of π -stacking play a particularly important role in this respect.^{3–5} From the wealth of previous studies it has emerged that D–A based CT compounds where the donors and the acceptors form segregated stacks (motif II in Fig. 2) show often higher charge mobilities than CT compounds where the donors and the acceptors form alternating (1:1 ratio) or mixed stacks ($n:1$ ratios) (motif I in Fig. 2). Illustrative examples are provided by various CT compounds assembled from TTF or its derivatives and TCNQ that crystallize in segregated D and A stacks and show conductivities of as high as 200 to 1000 S cm^{−1}.^{3,21} In contrast, CT compounds of tetramethoxyselenanthrenes and TCNQ form an alternately mixed-stacked structure [D⋯A]_∞ of type A–I and exhibit poor conductivities of 4 × 10^{−10} S cm^{−1}.^{3,21}

In this work, we have studied D–A compounds formed by combining the donors 2,2':6',2'':6'',6-trioxotriphenylamine (TOTA, Fig. 3) and a pyrene-annulated azaacene (PAA) with five different acceptors, namely the 2,3,5,6-tetrahalogeno-*p*-benzoquinones X₄BQ (X = F, Cl, Br), 2,3,5,6-tetrafluoro-7,7,8,8-tetracyanoquinodimethane (F₄TCNQ) and 7,7,8,8-tetracyanoquinodimethane (TCNQ). The donors constitute extended, planar π -systems and hence should be well-suited for π -stacking,^{23–25} but also allow for interdonor hydrogen bonding involving the O or N heteroatoms and for C≡N or C–F π -hole tetrel interactions.^{26–30} TOTA is a nonplanar, electron-rich molecule with a low half-wave potential $E_{1/2}^{0/+}$ of 110 mV (in CH₂Cl₂/NBu₄PF₆ against the ferrocene/ferrocenium standard couple FcH/FcH⁺ = 0 mV) for its first one-electron oxidation. In contrast, PAA shows its first oxidation potential at $E_{ox}^{0/+}$ = 1205 mV under the same experimental conditions and is hence a much weaker donor (Table 1, *vide infra*). The acceptors were

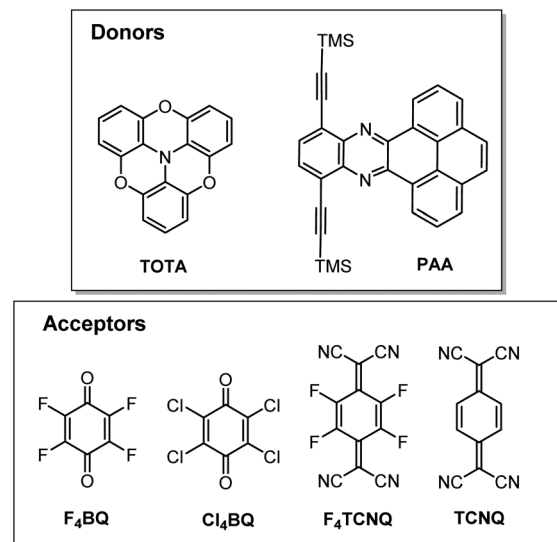


Fig. 3 The donors and acceptors used in this study.

chosen in order to cover a wider range of half-wave potentials for their first one-electron reduction, ranging from $E_{1/2}^{0/-}$ = 153 mV for F₄TCNQ to −464 mV for Cl₄BQ in the order F₄TCNQ > TCNQ > F₄BQ ≈ Cl₄BQ ≈ Br₄BQ (Table 1). We show that the degree of CT in the TOTA compounds varies considerably from the strong acceptor F₄TCNQ to the weaker acceptor F₄BQ as it is, *inter alia*, manifested by a structural change of the TOTA donor from bowl-shaped to planar with an increasing degree of CT. Almost no CT to F₄TCNQ was observed for the CT compound with the weaker PAA donor.

Results and discussion

Synthesis of the charge-transfer compounds

The D–A compounds formed on dissolving equimolar quantities of the respective pair of a donor and an acceptor in CH₂Cl₂ in a small vial. The vial was loosely capped by a screwcap and the solvent was allowed to slowly evaporate. After one or two weeks, dark purple crystals of a CT compound of TOTA and F₄TCNQ, dark orange crystals of a TOTA/F₄BQ and dark green crystals of a PAA/F₄TCNQ D–A compound were obtained. Other

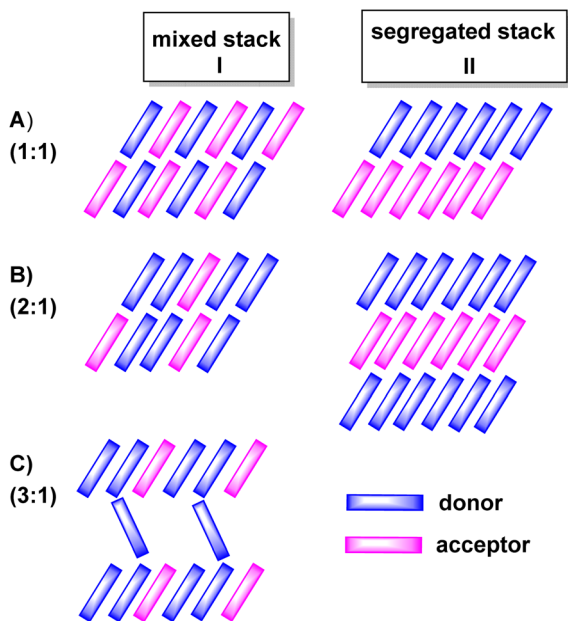


Fig. 2 Different stoichiometric ratios (top to bottom) and stacking motifs (left to right) commonly observed in charge-transfer (CT) compounds. (A) 1:1, (B) 2:1 and (C) 3:1 donor/acceptor or acceptor/donor ratios. Column I displays structures with mixed stacks and column II structures with segregated stacks.

Table 1 Cyclic voltammetry data of the donors and the acceptors of this study^a

	$E_{1/2}^{0/+}$	$E_{1/2}^{+/2+}$	$E_{1/2}^{0/-}$	$E_{1/2}^{-/2-}$
TOTA	110	1250	—	—
PAA	1205 ^b	—	−1590	—
F ₄ TCNQ	—	—	153	−484
TCNQ	—	—	−270	−850
F ₄ BQ	—	—	−448	−1336
Cl ₄ BQ	—	—	−452	−1236
Br ₄ BQ	—	—	−464	−1224

^a All data in millivolts *versus* FcH/FcH⁺ in CH₂Cl₂/NBu₄PF₆ at r. t. and at ν = 100 mV s^{−1}. ^b Peak potential of the forward peak of a chemically irreversible anodic wave.



combinations of one of these donors and another acceptor as well as using toluene as the solvent did not result in crystalline or phase-pure materials, although the formation of some pale-greenish crystals of a CT adduct of TOTA and TCNQ and of few yellow-green crystals from the PAA/TCNQ mixture were observed. These crystals did however not diffract well and could not be isolated in sufficient quantities and purity from the cocrystallized donor or acceptor to allow for their further investigation. Photographs of the three CT compounds discussed in this study and their precursors are provided in Fig. S1 in the ESI†


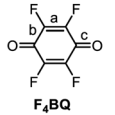
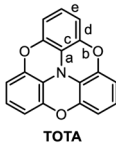
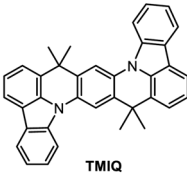
As discussed in the introduction, the electron donating and accepting abilities of all donors and acceptors were investigated by cyclic voltammetry. Representative cyclic voltammograms are provided in Fig. S2 to S4 in the ESI†; relevant data are listed in Table 1.

The TOTA-based CT compounds $(\text{TOTA})_2 \cdot (\text{F}_4\text{TCNQ})_2 \cdot \text{CH}_2\text{Cl}_2$ and $(\text{TOTA})_2 \cdot (\text{F}_4\text{BQ})$

2,2':6',2'':6'',6-Trioxotriphenylamine (TOTA) is slightly bowl-shaped and can be easily oxidized to a stable, planar radical cation.^{31,32} Its first oxidation potential $E_{1/2}^{0/+}$ of 110 mV against the ferrocene/ferrocenium standard (FcH/FcH^+) in $\text{CH}_2\text{Cl}_2/\text{Bu}_4\text{PF}_6$ (Bu_4PF_6 = tetrabutylammonium hexafluorophosphate) is close to the reported value of 140 mV in DMF.³¹ Its reaction with equimolar quantities of the strong acceptor F_4TCNQ accordingly yielded the 1:1 salt $(\text{TOTA})_2 \cdot (\text{F}_4\text{TCNQ})_2 \cdot \text{CH}_2\text{Cl}_2$ with an essentially full transfer of charge between the donor and the acceptor (*vide infra*). The compound crystallized in the monoclinic space group $P2_1/c$ with two crystallographically distinct molecules of the donor and the acceptor each and one CH_2Cl_2 solvent molecule in the unit cell. The structure is shown in Fig. 4.

The bond parameters of F_4TCNQ and, to a lesser extent, of TOTA are sensitive to their oxidation state. Neutral F_4TCNQ has a quinoid structure with pronounced short-long-short bond length alternation (see Fig. 3 and Table 2). One-electron reduction increases the aromaticity of the central ring and renders the intracyclic CC bonds more similar while

Table 2 Selected bond parameters of the CT compounds of this study and pertinent reference systems

	<i>a</i>	<i>b</i>	<i>c</i>	<i>d</i>	<i>e</i>	ref.
						
						
						
						
F_4TCNQ^a	1.337	1.439	1.372	1.437	—	33–36
$\text{F}_4\text{TCNQ}^{-a}$	1.358	1.417	1.418	1.430	1.385	37 and 38
TOTA	1.408	1.392	1.388	1.384	1.385	31
TOTA^{+a}	1.376	1.375	1.394	1.378	1.378	31 and 32
F_4BQ^a	1.339	1.477	1.213	—	—	39–41
Cl_4BQ	1.344	1.489	1.211	—	—	42
Cl_4BQ^-	1.360	1.448	1.248	—	—	43
$\text{TOTA} \cdot \text{F}_4\text{TCNQ}^b$	—	—	—	—	—	This work
TOTA	1.376	1.375	1.397	1.397	1.389	
F_4TCNQ	1.358	1.417	1.410	1.423	—	
$(\text{PAA})_4 \cdot \text{F}_4\text{TCNQ}$	1.341	1.445	1.381	1.443	—	This work
$(\text{TOTA})_2 \cdot \text{F}_4\text{BQ}$	1.402	1.390	1.389	1.386	1.393	This work
TOTA	1.336	1.472	1.219	—	—	
F_4BQ	1.328	1.470	1.212	—	—	44
$\text{TTF} \cdot \text{F}_4\text{BQ}$	1.316	1.470	1.210	—	—	45

^a Average values from different structures in the provided references. For F_4TCNQ^- , the data for the various crystallized NBu_4^+ salts and for TOTA^+ the data for the PF_6^- , ClO_4^- and ReO_4^- salts were used.
^b Average values for two crystallographically different donor and acceptor molecules in the unit cell.

lengthening the exocyclic $\text{C}=\text{C}$ bonds. This bond lengthening appears to constitute the most indicative structure change in tetracyanoquinodimethanes concomitant with reduction, which complies with the notion that the cyano groups are the primary electron acceptors.^{46–48} On the other hand, bond length changes on oxidation of TOTA are diluted over the entire polycyclic π -system so that the most indicative structural changes are the shortening of the N–C bonds and the flattening of the cone at the amine N atom from 10° to fully planar (see Fig. 5).

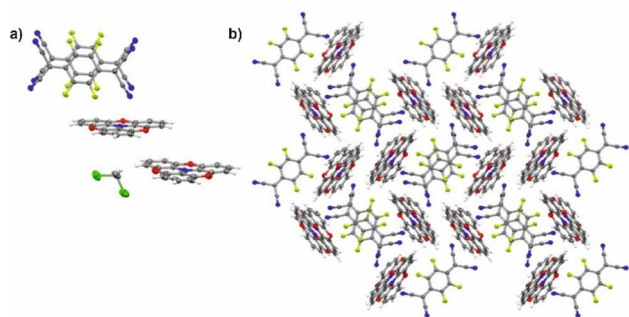


Fig. 4 X-ray structure of $(\text{TOTA})_2 \cdot (\text{F}_4\text{TCNQ})_2 \cdot \text{CH}_2\text{Cl}_2$. (a) Asymmetric unit showing the $(\text{F}_4\text{TCNQ}^-)_2$ dimer and the two crystallographically different TOTA^+ cations. (b) Packing motif of the donor and acceptor constituents in the crystal lattice; the CH_2Cl_2 solvent molecules are removed for clarity reasons. Colour codes: H, white; C, grey; N, blue; F, yellow-green; O, red; Cl, green.

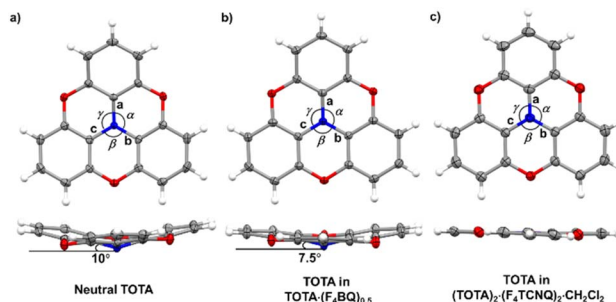


Fig. 5 X-ray structures and metric parameters of (a) neutral TOTA,³¹ (b) the TOTA constituent in $(\text{TOTA})_2 \cdot \text{F}_4\text{BQ}$ and (c) the TOTA^+ cation.



Table 2 summarizes pertinent bond lengths of reference compounds F_4TCNQ , F_4TCNQ^- , TOTA, $TOTA^+$, F_4BQ , Cl_4BQ , Cl_4BQ^- and the D–A compounds of the present study. As can be seen from the data in Table 2, the metrics of the TOTA and the F_4TCNQ constituents in $(TOTA)_2 \cdot (F_4TCNQ)_2 \cdot CH_2Cl_2$ agree with those of the $TOTA^+$ cation in the PF_6^- , ClO_4^- and ReO_4^- salts and of the F_4TCNQ^- anion in $NBu_4^+ F_4TCNQ^-$, respectively.^{37,38} In particular, the TOTA constituent has completely flattened out (Fig. 5c). This characterizes $(TOTA)_2 \cdot (F_4TCNQ)_2 \cdot CH_2Cl_2$ as a true CT salt with full ionicity.

In the crystal lattice, the F_4TCNQ^- anions associate to pairs of nearly parallel, eclipsed molecules with a tilt angle of 1.60° between their ring planes and a rather small interplanar distance of 3.215 \AA (Fig. 4 and 6). The formation of F_nTCNQ^- ($n = 0, 4$) dimers has been observed on previous occasions and is associated with an antiferromagnetic alignment of their unpaired spins.^{38,49–51} Individual $(F_4TCNQ^-)_2$ dimers are separated by two CH_2Cl_2 solvent molecules and arrange in columns that run parallel to the a axis of the unit cell. F_4TCNQ^- ions of neighbouring columns are nearly coplanar with a modest tilt of their ring planes by 6.7° and rotated by almost 90° .

The F_4TCNQ^- columns are separated by sheets that are formed by surrounding $TOTA^+$ cations. Like the F_4TCNQ^- anions, $TOTA^+$ polycycles that belong to different sheets adopt nearly orthogonal orientations with interplanar angles of 85.8° and 88.0° between their ring planes. As is shown in Fig. 4b, the F_4TCNQ^- dimers are engaged by six $TOTA^+$ cations and every TOTA cation is in turn surrounded by three F_4TCNQ^- dimers. This rather curious packing arrangement is established by various $C \equiv N \cdots$ and $C-F \cdots \pi$ -hole tetrel bonds^{26–30} as well as by $C-H \cdots N \equiv C$ hydrogen bonds and one weak $CH \cdots F$ interaction of 2.640 \AA . Fig. 6 provides a view of two neighbouring $(F_4TCNQ^-)_2(TOTA^+)_6$ cages with two additional weakly associated $TOTA^+$ cations and the ensuing network of noncovalent interactions. The $C \equiv N \cdots \pi$ -hole tetrel interactions range from 2.998

\AA to 3.183 \AA , while the $C-F \cdots \pi$ -hole contacts measure 2.977 \AA to 3.136 \AA ; $CH \cdots N$ interactions cover a range from 2.500 \AA to 2.701 \AA . Adjacent cages weakly associate by pairwise $CH \cdots O$ contacts of 2.697 \AA between parallel displaced and laterally offset $TOTA^+$ cations. When viewed along the b -axis of the unit cell (see the horizontal rows in Fig. 4b), an alternating arrangement of $(F_4TCNQ^-)_2$ π -dimers and two coplanar $TOTA^+$ cations emerges. The $D^+ \cdots D^+$ π - π interactions of 3.388 – 3.445 \AA are notably weaker than the $A^- \cdots A^-$ π - π interactions of 3.108 – 3.195 \AA (Fig. 4 and 6).

Single crystals of $(TOTA)_2 \cdot F_4BQ$ were grown by slow evaporation of a CH_2Cl_2 solution of their equimolar mixture. The asymmetric unit cell contains one TOTA donor molecule and half a F_4BQ acceptor molecule. In the crystal lattice, each F_4BQ acceptor molecule is surrounded by two slightly bowl-shaped TOTA donors to provide a centrosymmetric arrangement $D \cdots A \cdots D$ of nearly coplanar TOTA and F_4BQ molecules with interplanar angles of 3.6° between their planes as defined by the three oxygen atoms at the TOTA ether straps or the central C_6 ring of F_4BQ . The N atom of the TOTA donor is displaced by 0.25 \AA from the TOTA ring plane and points towards the F_4BQ acceptor to provide a $N \cdots F_4BQ_{\text{centr.}}$ distance of 2.851 \AA . These $D \cdots A \cdots D$ arrays stack into infinite columns that run along the c -axis of the unit cell. Fig. 7b provides a view of two such $D \cdots A \cdots D$ triples; an extended view over several unit cells down the c axis can be found as Fig. S5 of the ESI.† Neighbouring donors have an interplanar distance of 3.791 \AA between the centroids as defined by their oxygen atoms and form pairwise contacts $C5 \cdots C15$ of 3.238 \AA . Within the ab -plane of the unit cell, every F_4BQ acceptor associates with six coplanarly arranged TOTA donors through a total of eight $C-F \cdots H-C$ hydrogen bonds of 2.485 \AA to 2.643 \AA and four $O \cdots H-C$ hydrogen bonds of 2.567 \AA and 2.614 \AA , respectively (see Fig. S6 of the ESI†). The TOTA molecules that surround the F_4BQ acceptors connect through pairwise $O \cdots H-C$ hydrogen bonds of 2.656 \AA , respectively. In turn, every TOTA molecule is surrounded by alternately arranged TOTA donors

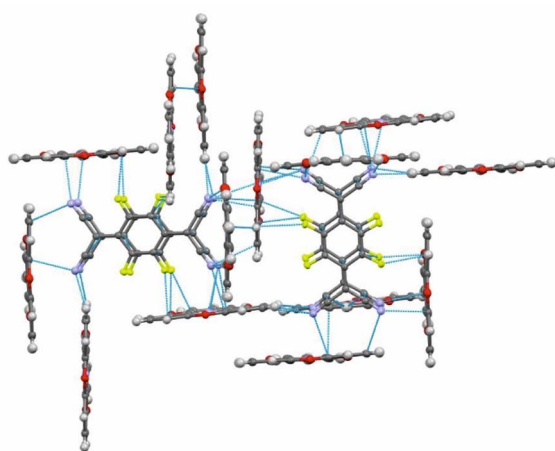


Fig. 6 Intermolecular π -stacking, $C \equiv N \cdots$ and $C-F \cdots \pi$ -hole tetrel and H-bonding interactions in $(TOTA)_2 \cdot (F_4TCNQ)_2 \cdot CH_2Cl_2$, distances shorter than the sum of the van der Waals radii are indicated by blue dotted lines.

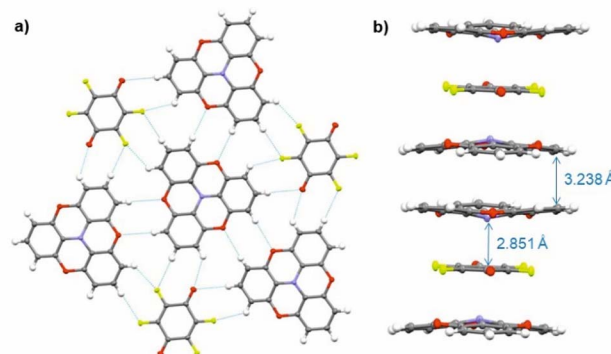


Fig. 7 X-ray molecular structure of $(TOTA)_2 \cdot F_4BQ$. (a) Packing diagram within the ab plane with intermolecular H-bonding interactions indicated by blue dotted lines. (b) One-dimensional $[D \cdots A \cdots D]_\infty$ columns that run along the c axis of the unit cell. Colour codes: H, white; C, grey; N, blue; F, yellow-green; O, red.



and F₄BQ acceptors. Fig. 7a provides a view of the molecule arrangement and the resulting H-bonding network.

The bonding parameters of both, the F₄BQ acceptor and the TOTA donor argue for an only limited degree of charge transfer, but do not allow for a quantitative assessment. Since no X-ray data for an authenticated F₄BQ[−] anion seem to be available in the literature, we resort to its chloro-substituted analogue Cl₄BQ^{*n*−} (*n* = 0, 1) for comparison.⁴³ One-electron reduction of Cl₄BQ causes a lengthening of the intracycle C=C bonds and, by a larger margin, the external C=O bonds while the former C–C bonds contract. The bond parameters of the F₄BQ constituent of (TOTA)₂·F₄BQ are close to that of F₄BQ itself or to those of its 1 : 1 TTF or its 1 : 2 TMIQ CT compounds, which also show only a fair degree of CT (TMIQ represents the 1,4-phenylene-bridged ditopic bis-carbazole donor shown on the right of the header of Table 2).^{44,45} In further agreement with an only modest degree of CT, the donor constituents retain the domed, non-planar structure of neutral TOTA, albeit with a smaller cone angle of 7.5° at the N atom and slightly wider C_{ph}–N–C_{ph} bond angles α , β , and γ of 116.57(10)°, 116.86(10)° and 117.00(10)° as compared to the values of 115.3(2)°, 115.6(2)° and 115.7(2)° for neutral TOTA (Fig. 5).³¹ As already mentioned, TOTA⁺ is planar with angles α , β , and γ close to 120° (e.g. 119.7(5)°, 119.9(5)° and 120.3(5)° in the perrhenate salt).²⁷ The N–C_{phenyl} and O–C_{phenyl} bond lengths in (TOTA)₂·F₄BQ are nearly identical to those of pristine, neutral TOTA and significantly longer than in (TOTA)₂·(F₄TCNQ)₂·CH₂Cl₂ or other salts with authenticated TOTA⁺ cations.^{31,32}

The donor-acceptor compound (PAA)₄·F₄TCNQ

As suggested by the high anodic peak potential of 1205 mV, the pyrene-annulated azaacene PAA (Fig. 3) is only a very poor donor. Hence, the formation of a binary D–A compound was only observed with the strongest acceptor F₄TCNQ. The dark green crystals obtained by slow evaporation of CH₂Cl₂ from a 1 : 1 solution of PAA and F₄TCNQ turned out to assume a rather unusual 4 : 1 D : A stoichiometry (PAA)₄·F₄TCNQ. The compound crystallized in the monoclinic space group *C2/c*. The asymmetric unit consists of two molecules of the PAA donor and half a molecule of the F₄TCNQ acceptor. In the crystal lattice, repeat units of four D and one A molecules form one-dimensional infinite columns [...D...D...A...D...D...]∞ that run along alternately the *a* or the *b* axis of the unit cell (Fig. 8). The neighbouring, crystallographically unique PAA donors PAA1 and PAA2 of an A...D...D... sequence align in a quasi-centrosymmetric fashion in order to minimize steric repulsion between the bulky trimethylsilyl substituents. As is shown in the left panel of Fig. 8, these building blocks repeat in a centrosymmetric manner to generate columns. With inter-plane angles F₄TCNQ–PAA1 of 2.30° and PAA1–PAA2 of 1.96°, the individual donor and the acceptor molecules arrange in a nearly coplanar fashion. Separations of 3.324 Å (F₄TCNQ–PAA1), 3.328 Å (PAA1–PAA2) and 3.378 Å (PAA2–PAA2) are all smaller than 3.5 Å, which indicates π -stacking interactions.⁵²

The close match between the bond lengths of the A constituent of this compound to those of neutral F₄TCNQ evidences

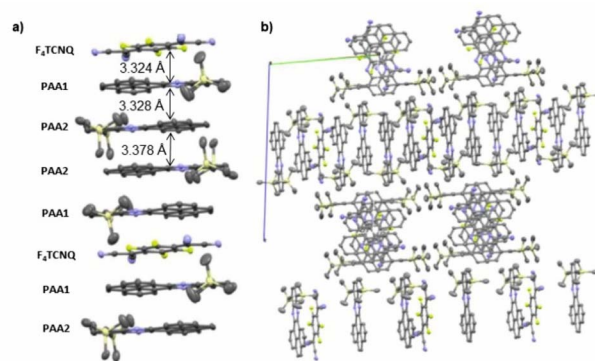


Fig. 8 (a) Molecular packing of (PAA)₄·F₄TCNQ viewed along the *a* axis of the unit cell. (b) Alignment of the rows in the crystal lattice. Solvent molecules are removed for clarity reasons.

the lack of any substantial degree of CT from PAA. The bonding parameters of the crystallographically distinct PAA donors in (PAA)₄·F₄TCNQ differ slightly (see Fig. S7 of the ESI†), but are in line with those in neutral, pyrene-appended azaacene derivatives and other bis(trimethylsilyl) derivatives of diethynyl-substituted azaacenes.^{23,24}

As a bottom line, crystallographic data indicate full CT in (TOTA)₂·(F₄TCNQ)₂, an only moderate degree of CT in (TOTA)₂·F₄BQ, and the absence of any significant degree of CT in (PAA)₄·F₄TCNQ, which complies with the difference of oxidation potentials of the respective donor and the reduction potential of the acceptor.

IR, UV-vis-NIR and EPR spectroscopy

In addition to structure data, infrared (IR) and UV-vis-NIR spectroscopy have proven highly instructive for quantifying the extent of charge-transfer in D–A compounds. Of particular diagnostic value are the redox state-dependent band positions of the nitrile C≡N $\tilde{\nu}$ (CN) or the quinone C=O stretching modes $\tilde{\nu}$ (CO) of the acceptor. Their shift with respect to the neutral and the reduced forms of the respective acceptor scales linearly with the fraction of charge ρ (in units of the elementary charge *e*) transferred from the donor to the acceptor.^{53,54} These band shifts provide a widely applied criterion for assessing the degree of CT.^{6,21,55–60} Arene stretching and bending vibrations of the D component may provide additional information.

The CN stretches of the F₄TCNQ acceptor in TOTA·F₄TCNQ at $\tilde{\nu}$ = 2196 cm^{−1} and 2176 cm^{−1} are significantly red-shifted from their positions of 2227 cm^{−1} (the stronger *b*_{1u} mode) and 2212 cm^{−1} (the weaker *b*_{2u} mode) in pristine F₄TCNQ (Fig. 9a)⁶¹ and closely resemble those of the F₄TCNQ[−] anion of 2194 cm^{−1} and 2172 cm^{−1}.^{6,61,62} The degree of charge-transfer ρ to F₄TCNQ can be calculated according to eqn (1),

$$\rho = (2 \cdot \Delta\tilde{\nu}/\tilde{\nu}_0) \cdot (1 - \tilde{\nu}_{-1}^2/\tilde{\nu}_0^2)^{-1} \quad (\text{ref. 6 and 54}) \quad (1)$$

where $\tilde{\nu}_0$ and $\tilde{\nu}_{-1}$ represent the wavenumber of the more prominent C≡N stretching vibration in neutral F₄TCNQ ($\tilde{\nu}_0$) or its associated radical anion ($\tilde{\nu}_{-1}$), and $\Delta\tilde{\nu}$ is the difference between



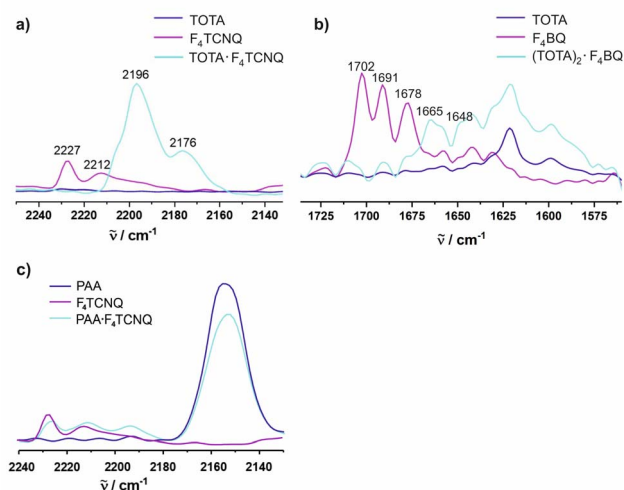


Fig. 9 Spectroscopic changes in the mid IR region (C≡N stretching vibrations) of F₄TCNQ in (a) (TOTA)₂·(F₄TCNQ)₂·CH₂Cl₂, (b) (TOTA)₂·F₄BQ, and (c) (PAA)₄·F₄TCNQ.

the band position in neutral F₄TCNQ and the charge transfer compound, $\tilde{\nu}_0 - \tilde{\nu}_{CT}$, respectively. Applying eqn (1) to TOTA·F₄TCNQ yields $\rho = 0.95$ in agreement with essentially full electron transfer. IR data for the D constituent agree with this view. Hence, IR(KBr) spectra of TOTA·F₄TCNQ feature donor bands at 1590, 1334, 1277, 1074 and 1031 cm⁻¹ (see Fig. S8 of the ESI†). These values are nearly identical to those of 1589, 1333, 1275, 1072 and 1028 cm⁻¹ reported in the literature for the TOTA⁺ radical cation and differ from those of pristine TOTA (1621, 1480, 1336, 1318, 1265, 1067 and 1018 cm⁻¹).⁶³

The formation of D–A compounds is also evident from UV-vis-NIR spectroscopy. UV-vis-NIR spectra of solid samples of neutral TOTA and F₄TCNQ and of the CT compound TOTA·F₄TCNQ were recorded in an integrating sphere in order to diminish intensity losses due to scattering and reflection. As shown in Fig. 10, the spectra of the neutral precursors display intense bands at 380 and 525 nm and 405 and 455 nm, respectively, whereas TOTA·F₄TCNQ shows discernible peaks at 595, 650, 770 and at *ca.* 1060 nm.

EPR spectroscopy provides a highly sensitive probe of paramagnetic species resulting from charge transfer.^{62,64,65} Solid

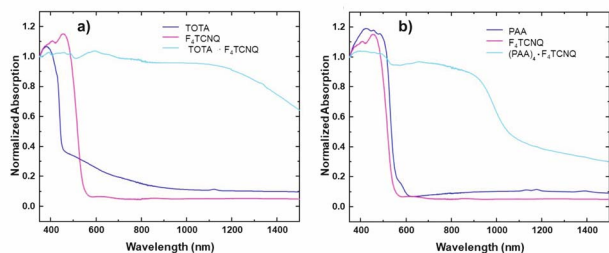


Fig. 10 Monitoring the CT compound formation by UV-vis-NIR spectroscopy. The spectra of CT compounds are plotted with their parent donor and acceptor constituents. (a) (TOTA)₂·(F₄TCNQ)₂·CH₂Cl₂ and (b) (PAA)₄(F₄TCNQ).

TOTA·F₄TCNQ (Fig. 11a) shows accordingly an intense EPR resonance at a *g* value of 1.9990, whose intensity increases on cooling. This agrees with the *T*-dependent Boltzmann distribution as given in eqn (2)^{66,67} and the high ionicity in the ground state of this compound. One should note here that the observed EPR resonance in the solid state is likely due to exclusively the TOTA⁺ cation, as the F₄TCNQ⁻ anions associate to diamagnetic dimers.

$$\Delta N \approx N \cdot \frac{g \cdot \mu_B \cdot B_0}{2k_B T} \quad (2)$$

For F₄BQ, the energies of the $\nu(\text{CO})$ stretching vibrations serve the same purpose as the CN bands in X_nTCNQ derivatives (X = Hal, *n* = 0–4) such that eqn (1) applies accordingly. ν_{CO} bands of F₄BQ in (TOTA)₂·F₄BQ are found at 1665 and 1648 cm⁻¹, whereas they are located at 1702, 1691 and 1678 cm⁻¹ in neutral F₄BQ (see Fig. 9b). The data are to be compared with literature values of 1705, 1693 and 1686 cm⁻¹ for F₄BQ⁶⁸ and 1556 and 1502 cm⁻¹ for the sodium salt of F₄BQ^{69,70}. Using eqn (1), ρ was calculated as 0.26. Hence, (TOTA)₂·F₄BQ seems to exhibit a fair degree of CT which was not so evident from the structure data. There are only minor shifts in the IR bands of the TOTA constituents (Fig. S9 of the ESI†). One should, however, note that the extent of charge loss from an individual TOTA donor is only half of that which is accumulated at the F₄BQ acceptor. In the solid state, (TOTA)₂·F₄BQ exhibits a weak, broad CT absorption at low energy (Fig. S10 of the ESI†). As shown in Fig. 11b, solid TOTA·F₄BQ is also EPR active, but shows an opposite *T* dependence to TOTA·F₄TCNQ, i. e. the signal intensity decreases on lowering the temperature. This suggests that CT in these compounds is a thermally activated process. In summary, IR, UV-vis-NIR and EPR data on the solid samples are consistent with the notion of (nearly) quantitative CT from the donor to the acceptor in TOTA·F₄TCNQ and a more modest one in (TOTA)₂·F₄BQ. The degree of CT ρ as quantified by the shift of the C≡N stretching vibrations of the donor amounts to 0.95 and 0.26, respectively.

In contrast, the IR data of (PAA)₄(F₄TCNQ) resemble those of the pristine, neutral constituents closely with only a small shift of the ν_{CN} band by *ca.* 1.5 cm⁻¹ (Fig. 9c) which translates into $\rho \approx 0.05$, thus indicating a very modest degree of CT (see also Fig. S11 of the ESI† for the arene bands). In agreement with the small degree of CT, (PAA)₄(F₄TCNQ) shows only a very weak EPR

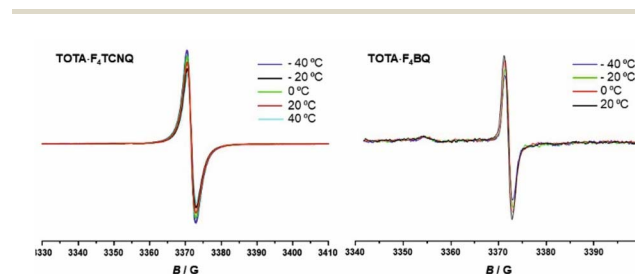


Fig. 11 *T*-dependent EPR spectra of the CT compounds TOTA·F₄TCNQ (left) and (TOTA)₂·F₄BQ (right).



resonance signal (see Fig. S12 of the ESI†). Nevertheless, the compound absorbs strongly in the solid state over the entire UV and vis range down to 1100 nm as shown in Fig. 10b. We note that accounts of compounds showing prominent CT bands despite small degrees of CT have appeared in the literature.¹⁹

In order to assess their conductive properties, single crystals of all three isolated CT compounds were placed on a gold plate or a conductive Cu-tape and contacted with two closely spaced nanoprobe, which served as electrodes (for details to the experimental setup, see the Materials and methods section and Fig. S13 of the ESI†). Even on applying a maximum voltage of 20 V, no detectable current flow was observed for TOTA·F₄TCNQ and for (PAA)₄·F₄TCNQ, even at a tip distance as small as *ca.* 10 μm. Their insulating behaviour (Fig. S14 and S15 of the ESI†) is a direct consequence of their structures with very weakly interacting (TOTA)⁺₈(F₄TCNQ[−])₂ cages or [···D···D···A···D···D···]_∞ columns with negligible charge transfer. (TOTA)₂·F₄BQ is also nearly insulating with a resistance per unit length of 5–10 GΩ μm^{−1} for different specimen, which is close to the detection limit of our experimental setup (Fig. S16–S19 of the ESI†).

Conclusions

We describe two charge-transfer compounds of the 2,2′:6′,2′′:6′,6′-trioxotriphenylamine donor and tetrafluoro-tetracyano-*p*-quinodimethane (F₄TCNQ) or tetrafluoro-*p*-benzoquinone (F₄BQ) as the acceptor component and a donor-acceptor complex of a much less electron-rich pyrene-annulated azaacene (PAA) with F₄TCNQ. Although in each case equimolar amounts of the donor D and the acceptor A were used for their synthesis, only (TOTA)₂·(F₄TCNQ)₂·CH₂Cl₂ adopted a D:A stoichiometry of 1:1. Crystals isolated with F₄BQ as the acceptor provided a 2:1 ratio between the donor and the acceptor constituents instead. The combination of PAA and F₄TCNQ resulted even in a rare 4:1 composition, yielding (PAA)₄·(F₄TCNQ). X-ray diffraction analysis indicated full charge transfer from the donor to the acceptor in (TOTA)₂·(F₄TCNQ)₂·CH₂Cl₂ by virtue of the bond parameters of the F₄TCNQ acceptor and the planarization of the TOTA constituent. These findings are also supported by IR and UV-vis-NIR spectroscopy. In the crystalline state, π-stacked F₄TCNQ[−] dimers are encaged by six TOTA⁺ counterions with only weak interactions between these structural entities.

For the other two D/A combinations, X-ray structure analysis revealed mixed stacking patterns with [D···A···D]_∞ or [D···D···A···D···D]_∞ packing motifs. Monitoring the shifts of the C≡N and C=O stretching frequencies in the CT compounds with respect to the neutral and monoreduced acceptors revealed an essentially complete charge-transfer in (TOTA)₂·(F₄TCNQ)₂·CH₂Cl₂, a moderate degree of charge-transfer in (TOTA)₂·(F₄BQ) (*ρ* = 0.26) and an only very modest degree of CT in (PAA)₄·(F₄TCNQ). Nevertheless, a fairly intense CT band was found in solid state UV-vis-NIR spectra. *T*-dependent EPR spectra recorded in the solid state agree with a (nearly) complete CT in the ground state of the TOTA·F₄TCNQ compound, while CT in (TOTA)₂·(F₄BQ) is thermally activated and (PAA)₄·(F₄TCNQ) shows only a very weak EPR signal. All CT compounds are non-conductive or, in the case of (TOTA)₂·(F₄BQ) very weakly conductive in the solid state.

Data availability

Details to the methods and materials, characterization data and additional figures can be found in the ESI†. CCDC reference numbers for the reported crystallographic structures are 2220394 ((PAA)₄·F₄TCNQ), 2220397 ((TOTA)₂·F₄BQ) and 2220398 ((TOTA)₂·(F₄TCNQ)₂·CH₂Cl₂).

Conflicts of interest

There are no conflicts to declare.

Acknowledgements

We are indebted to the German Research Foundation (Deutsche Forschungsgemeinschaft, DFG) for financial support of this work through grant Wi1262/17-1.

Notes and references

- 1 J. Ferraris, D. O. Cowan, J. V. Walatka and J. H. Perlstein, *J. Am. Chem. Soc.*, 1973, **95**, 948–949.
- 2 H. Bassler and A. Kohler, *Top. Curr. Chem.*, 2012, **312**, 1–65.
- 3 K. P. Goetz, D. Vermeulen, M. E. Payne, C. Kloc, L. E. McNeil and O. D. Jurchescu, *J. Mater. Chem. C*, 2014, **2**, 3065–3076.
- 4 J. Zhang, W. Xu, P. Sheng, G. Zhao and D. Zhu, *Acc. Chem. Res.*, 2017, **50**, 1654–1662.
- 5 W. Wang, L. Luo, P. Sheng, J. Zhang and Q. Zhang, *Chem.–Eur. J.*, 2021, **27**, 464–490.
- 6 B. Mahns, O. Kataeva, D. Islamov, S. Hampel, F. Steckel, C. Hess, M. Knupfer, B. Büchner, C. Himcinschi, T. Hahn, R. Renger and J. Kortus, *Cryst. Growth Des.*, 2014, **14**, 1338–1346.
- 7 L. Zhu, H. Geng, Y. Yi and Z. Wei, *Phys. Chem. Chem. Phys.*, 2017, **19**, 4418–4425.
- 8 J. Singleton, *J. Solid State Chem.*, 2002, **168**, 675–689.
- 9 J. Zhang, H. Geng, T. S. Virk, Y. Zhao, J. Tan, C.-a. Di, W. Xu, K. Singh, W. Hu, Z. Shuai, Y. Liu and D. Zhu, *Adv. Mater.*, 2012, **24**, 2603–2607.
- 10 T. Wakahara, P. D'Angelo, K. i. Miyazawa, Y. Nemoto, O. Ito, N. Tanigaki, D. D. C. Bradley and T. D. Anthopoulos, *J. Am. Chem. Soc.*, 2012, **134**, 7204–7206.
- 11 W. Yu, X.-Y. Wang, J. Li, Z.-T. Li, Y.-K. Yan, W. Wang and J. Pei, *Chem. Commun.*, 2013, **49**, 54–56.
- 12 H.-D. Wu, F.-X. Wang, Y. Xiao and G.-B. Pan, *J. Mater. Chem. C*, 2014, **2**, 2328–2332.
- 13 S. J. Kang, J. B. Kim, C.-Y. Chiu, S. Ahn, T. Schiros, S. S. Lee, K. G. Yager, M. F. Toney, Y.-L. Loo and C. Nuckolls, *Angew. Chem., Int. Ed.*, 2012, **51**, 8594–8597.
- 14 P.-M. Allemand, K. C. Khemani, A. Koch, F. Wudl, K. Holzer, S. Donovan, G. Grüner and J. D. Thompson, *Science*, 1991, **253**, 301–302.
- 15 T. Enoki and A. Miyazaki, *Chem. Rev.*, 2004, **104**, 5449–5477.
- 16 Y. L. Lei, Y. Jin, D. Y. Zhou, W. Gu, X. B. Shi, L. S. Liao and S. T. Lee, *Adv. Mater.*, 2012, **24**, 5345–5351.
- 17 Y. L. Lei, L. S. Liao and S. T. Lee, *J. Am. Chem. Soc.*, 2013, **135**, 3744–3747.



- 18 W. Zhu, R. Zheng, X. Fu, H. Fu, Q. Shi, Y. Zhen, H. Dong and W. Hu, *Angew. Chem., Int. Ed.*, 2015, **54**, 6785–6789.
- 19 Y. Sun, Y. Lei, L. Liao and W. Hu, *Angew. Chem., Int. Ed.*, 2017, **56**, 10352–10356.
- 20 I. Salzmann, G. Heimel, M. Oehzelt, S. Winkler and N. Koch, *Acc. Chem. Res.*, 2016, **49**, 370–378.
- 21 H. Jiang, P. Hu, J. Ye, K. K. Zhang, Y. Long, W. Hu and C. Kloc, *J. Mater. Chem. C*, 2018, **6**, 1884–1902.
- 22 R. J. Walwyn, B. Chan, P. M. Usov, M. B. Solomon, S. G. Duyker, J. Y. Koo, M. Kawano, P. Turner, C. J. Kepert and D. M. D'Alessandro, *J. Mater. Chem. C*, 2018, **6**, 1092–1104.
- 23 P. Biegger, S. Stolz, S. N. Intorp, Y. Zhang, J. U. Engelhart, F. Rominger, K. I. Hardcastle, U. Lemmer, X. Qian, M. Hamburger and U. H. F. Bunz, *J. Org. Chem.*, 2015, **80**, 582–589.
- 24 X. Yu, J. Wan, C. Yuan, N. Guo, Y. Shen and J. Li, *Dyes Pigm.*, 2019, **161**, 130–136.
- 25 B. D. Lindner, Y. Zhang, S. Höfle, N. Berger, C. Teusch, M. Jesper, K. I. Hardcastle, X. Qian, U. Lemmer, A. Colsmann, U. H. F. Bunz and M. Hamburger, *J. Mater. Chem. C*, 2013, **1**, 5718–5724.
- 26 S. Scheiner, *Phys. Chem. Chem. Phys.*, 2021, **23**, 5702–5717.
- 27 A. M. Montana, *ChemistrySelect*, 2017, **2**, 9094–9112.
- 28 S. J. Grabowski, *Molecules*, 2021, **26**, 4939.
- 29 S. M. Nashre-ul-Islam, K. K. Borah, F. E. Ozturkkan, M. A. Raza, A. Frontera and D. M. Gil, *J. Mol. Struct.*, 2022, **1268**, 133686.
- 30 S. Scheiner, *Molecules*, 2020, **25**, 4495.
- 31 M. Kuratsu, M. Kozaki and K. Okada, *Angew. Chem., Int. Ed.*, 2005, **44**, 4056–4058.
- 32 Y. Nakano, H. Yamochi, G. Saito, M. Kuratsu and K. Okada, *J. Phys.: Conf. Ser.*, 2008, **132**, 012024.
- 33 T. J. Emge, M. Maxfield, D. O. Cowan and T. J. Kistenmacher, *Mol. Cryst. Liq. Cryst.*, 1981, **65**, 161–178.
- 34 Y. Krupskaya, M. Gibertini, N. Marzari and A. F. Morpurgo, *Adv. Mater.*, 2015, **27**, 2453–2458.
- 35 T. Salzillo, M. Masino, G. Kociok-Köhn, D. Di Nuzzo, E. Venuti, R. G. Della Valle, D. Vanossi, C. Fontanesi, A. Girlando, A. Brillante and E. Da Como, *Cryst. Growth Des.*, 2016, **16**, 3028–3036.
- 36 R. Shukla, C. Ruzie, G. Schweicher, A. R. Kennedy, Y. H. Geerts, D. Chopra and B. Chattopadhyay, *Acta Crystallogr., Sect. B: Struct. Sci., Cryst. Eng. Mater.*, 2019, **75**, 71–78.
- 37 J. S. Park, J. Park, Y. J. Yang, T. T. Tran, I. S. Kim and J. L. Sessler, *J. Am. Chem. Soc.*, 2018, **140**, 7598–7604.
- 38 S. A. O'Kane, R. Clérac, H. Zhao, X. Ouyang, J. R. Galán-Mascarós, R. Heintz and K. R. Dunbar, *J. Solid State Chem.*, 2000, **152**, 159–173.
- 39 R. Shukla and D. Chopra, *CrystEngComm*, 2018, **20**, 3308–3312.
- 40 K. Hagen, D. G. Nicholson and L. J. Saethre, *Acta Crystallogr., Sect. C: Cryst. Struct. Commun.*, 1987, **43**, 1959–1961.
- 41 A. Meresse, C. Courseille and B. C. Nguyen, *Acta Crystallogr., Sect. B: Struct. Sci., Cryst. Eng. Mater.*, 1974, **30**, 524–526.
- 42 K. J. Van Weperen and G. J. Visser, *Acta Crystallogr., Sect. B: Struct. Sci., Cryst. Eng. Mater.*, 1972, **28**, 338–342.
- 43 J.-M. Lü, S. V. Rosokha, I. S. Neretin and J. K. Kochi, *J. Am. Chem. Soc.*, 2006, **128**, 16708–16719.
- 44 J. J. Mayerle, J. B. Torrance and J. I. Crowley, *Acta Crystallogr., Sect. B: Struct. Sci., Cryst. Eng. Mater.*, 1979, **35**, 2988–2995.
- 45 Z. Wang, F. Yu, J. Xie, J. Zhao, Y. Zou, Z. Wang and Q. Zhang, *Chem.–Eur. J.*, 2020, **26**, 3578–3585.
- 46 E. Espinosa, E. Molins and C. Lecomte, *Phys. Rev. B: Condens. Matter Mater. Phys.*, 1997, **56**, 1820–1833.
- 47 P. Coppens, T. N. Guru Row, P. Leung, E. D. Stevens, P. J. Becker and Y. W. Yang, *Acta Crystallogr., Sect. A: Cryst. Phys., Diff., Theor. Gen. Crystallogr.*, 1979, **35**, 63–72.
- 48 P. Coppens, *Phys. Rev. Lett.*, 1975, **35**, 98–100.
- 49 R. H. Harms, H. J. Keller, D. Noethe, D. Wehe, N. Heimer, R. M. Metzger, D. Gundel and H. Sixl, *Mol. Cryst. Liq. Cryst.*, 1982, **85**, 1639–1645.
- 50 A. L. Sutton, B. F. Abrahams, D. M. D'Alessandro, T. A. Hudson, R. Robson and P. M. Usov, *CrystEngComm*, 2016, **18**, 8906–8914.
- 51 O. J. Dautel and M. Fourmigué, *New J. Chem.*, 2001, **25**, 834–838.
- 52 A. Bondi, *J. Phys. Chem.*, 1964, **68**, 441–451.
- 53 J. S. Chappell, A. N. Bloch, W. A. Bryden, M. Maxfield, T. O. Poehler and D. O. Cowan, *J. Am. Chem. Soc.*, 1981, **103**, 2442–2443.
- 54 A. Salmerón-Valverde, J. G. Robles-Martínez and A. Zehe, *Cryst. Res. Technol.*, 1994, **29**, 703–706.
- 55 M. Rudloff, K. Ackermann, M. Huth, H. O. Jeschke, M. Tomic, R. Valenti, B. Wolfram, M. Bröring, M. Bolte, D. Chercka, M. Baumgarten and K. Müllen, *Phys. Chem. Chem. Phys.*, 2015, **17**, 4118–4126.
- 56 A. Morherr, S. Witt, A. Chernenkaya, J.-P. Bäcker, G. Schönhense, M. Bolte and C. Krellner, *Phys. Rev. B*, 2016, **496**, 98–105.
- 57 P. Hu, K. Du, F. Wei, H. Jiang and C. Kloc, *Cryst. Growth Des.*, 2016, **16**, 3019–3027.
- 58 P. Hu, H. Li, Y. Li, H. Jiang and C. Kloc, *CrystEngComm*, 2017, **19**, 618–624.
- 59 O. Kataeva, M. Nohr, K. Ivshin, S. Hampel, B. Büchner and M. Knupfer, *Cryst. Growth Des.*, 2021, **21**, 471–481.
- 60 N. R. Goud and A. J. Matzger, *Cryst. Growth Des.*, 2016, **17**, 328–336.
- 61 M. Meneghetti and C. Pecile, *J. Chem. Phys.*, 1986, **84**, 4149–4162.
- 62 R. Das, M. Linseis, S. M. Schupp, L. Schmidt-Mende and R. F. Winter, *Chem.–Eur. J.*, 2022, **28**, e202104403.
- 63 M. Kuratsu, S. Suzuki, M. Kozaki, D. Shiomi, K. Sato, T. Takui and K. Okada, *Inorg. Chem.*, 2007, **46**, 10153–10157.
- 64 R. Das, M. Linseis, L. Senft, I. Ivanović-Burmazović and R. F. Winter, *Inorganics*, 2022, **10**, 82.
- 65 R. Das, M. Linseis, S. Scheerer, K. Zoller, L. Senft, I. Ivanović-Burmazović and R. F. Winter, *Inorg. Chem.*, 2022, **61**, 12662–12677.
- 66 G. R. Eaton, S. S. Eaton, D. Barr and R. T. Weber, *Quantitative EPR: A Practitioner's Guide*, Springer Verlag, Vienna, 1st edn, 2010.



- 67 C. Corvaja, *Electron Paramagnetic Resonance - A Practitioner's Toolkit*, Wiley VCH Verlag GmbH & Co, Hoboken, New Jersey, 2009.
- 68 A. Girlando and C. Pecile, *J. Chem. Soc., Faraday Trans. 2*, 1975, **71**, 689–698.
- 69 S. E. Boesch and R. A. Wheeler, *J. Phys. Chem. A*, 1997, **101**, 8351–8359.
- 70 G. Balakrishnan, P. Mohandas and S. Umapathy, *J. Phys. Chem. A*, 2001, **105**, 7778–7789.

